CRYSTAL GROWTH & DESIGN

pubs.acs.org/crystal

Article

Synthesis of Millimeter-Sized Spherical Ferrierite Zeolite by Vapor-Assisted Conversion

Published as part of a Crystal Growth and Design virtual special issue on Zeolite Crystal Engineering

Lingyun Li, Quanyi Wang, Dong Fan, Miao Yang, Peng Tian,* and Zhongmin Liu*

Cite This: *Cryst. Growth Des.* 2023, 23, 1951−1958

Read Online

ACCESS | Metrics & More | Article Recommendations

ABSTRACT: A facile vapor-assisted conversion strategy has been developed to prepare mechanically robust spherical ferrierite zeolite, in which millimeter-sized commercial silica spheres doped with Na and Al were utilized as the precursor and cheap ethylenediamine (EDA) aqueous solution as the liquid phase. Characterization results demonstrated that the shape of the spheres can be well maintained after crystallization, and their interior is solid with compact crystal intergrowth. The ferrierite content in the resultant spheres can reach as high as 100%. More interestingly, the as-synthesized ferrierite spheres are Na^+-free, and proton-form product can be directly obtained after simple calcination. The crystallization process of spherical ferrierite and the influence factors on the synthesis were investigated. It was revealed that control of the Na amount on the spherical precursor was critical for the crystallization, and a Na/Si ratio in the range of 0.10−0.13 facilitated the achievement of binder-free ferrierite spheres.

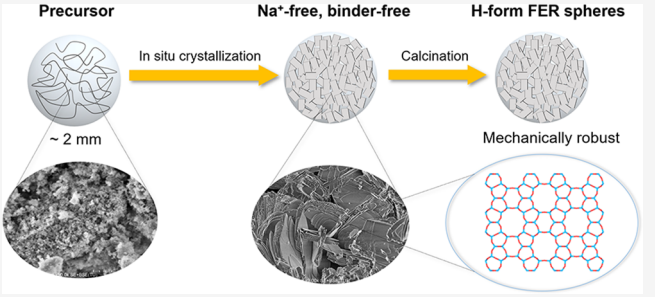

1. INTRODUCTION

Aluminosilicate zeolites are important crystalline microporous materials, which have found widespread applications in the chemical industry including catalysis, adsorption, separation, etc. Ferrierite (also denoted as ZSM-35) is one of the important members of the zeolite family, which possesses a two-dimensional framework consisting of an intersected 8-membered ring (8-MR) and 10-MR channels and has good (hydro)thermal stability.[1,2] Ferrierite has exhibited excellent catalytic activity in *n*-alkene skeletal isomerization,[3] dimethyl ether carbonylation,[4] and olefin oligomerization to diesel.[5] When combined with other components, the catalytic applications of ferrierite can be further extended. For example, Cu-ZnO-Al_2O_3/ferrierite composites were reported to be superior catalysts for syngas conversion to dimethyl ether.[6] Pt/ferrierite showed good catalytic performance in the selective catalytic reduction of NO by H_2 with high NO conversion and N_2 selectivity.[7]

Over the past few decades, the research on the synthesis of ferrierite mainly focuses on the control of crystal morphology,[5,8,9] the development of new organic structure directing agents (OSDAs)[10−13] and new synthetic routes,[14−16] and the tuning of the Al location (acid distribution) in the framework.[10,17−20] Plank et al. first reported the hydrothermal synthesis of ferrierite in 1977.[21] Xu et al. subsequently synthesized ferrierite in a nonaqueous system and revealed that its crystallization followed a solid phase transformation mechanism.[22] To decrease the diffusion lengths along the 10-MR direction, nanoneedle-like ferrierite was synthesized by using choline or pyrrolidine as OSDA, which can effectively improve the catalytic activity of 1-butene skeletal isomerization.[8,23] Pinar et al. reported the synthesis of ferrierite in a fluoride-assisted system.[24] They also revealed the distribution of Brønsted acid sites in ferrierite depends on the OSDA used. For example, in an HF-pyrrolidine-tetramethylammonium system, the acid sites are mainly distributed at the 8-MR pore mouths, while in an HF-pyrrolidine system, the Brønsted acid sites are distributed in the fer cages.[10]

Nevertheless, the synthesized zeolites in powder form need to go through other multisteps, such as calcination to remove OSDAs, ion exchange, shaping and calcination again to obtain proton-form products, before they can be loaded into industrial reactors. The shaping process is necessary to prepare zeolite catalysts with a suitable shape/size and sufficient mechanical strength, in order to avoid the large pressure drop of the reactors and ensure their long-term use of the catalyst

Received: December 14, 2022
Revised: January 29, 2023
Published: February 6, 2023

https://doi.org/10.1021/acs.cgd.2c01486
Cryst. Growth Des. 2023, 23, 1951−1958

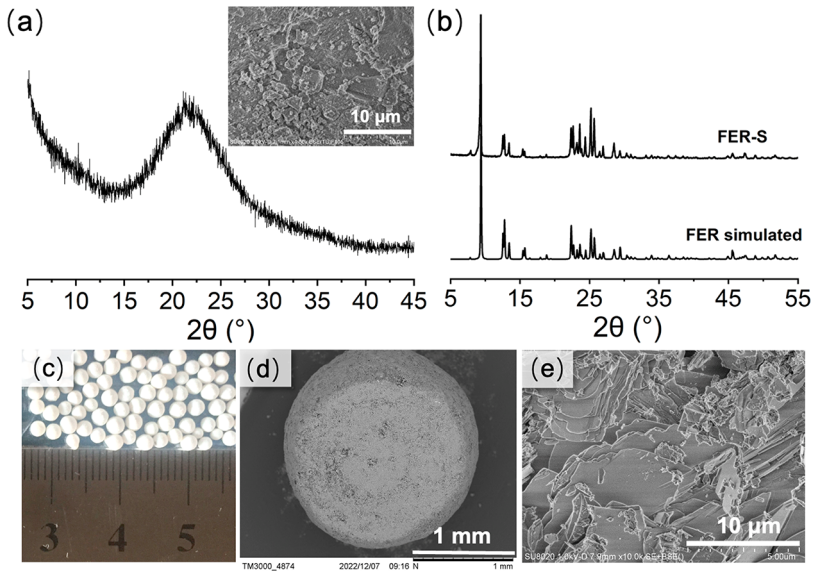

Figure 1. XRD patterns of a silica sphere (a) and as-synthesized spherical FER-S (b), optical photograph (c), SEM images of the cross-section (d) and internal crystals (e) of spherical FER-S. The inset SEM image in (a) shows the interior of a silica sphere.

with less powdering. Binders are generally indispensable for the shaping process of zeolite catalysts, which include water glass, clay, silica sol, alumina, etc. As the inorganic binders cannot be removed by calcination, their introduction reduces the content of active components. Moreover, they may block the pore mouth of zeolites, causing aggravated mass transfer limitation. Therefore, it would be desirable to synthesize binder-free zeolites with a specific shape/size and good mechanical strength.

The strategies developed for the preparation of binder-free zeolite catalysts include 3D printing,[25−27] pressure shaping,[28] gel casting,[29] and self-assembly of nanosized zeolites.[30] However, the relevant preparation procedures are generally complicated, and the products often have limited mechanical strength. Another method is the in situ crystallization of preshaped precursors prepared by mixing raw amorphous materials and shaping them into a certain shape and size. As the diameter of the catalyst particles used for industrial fixed-bed reactors is generally in the size of millimeters, it is critical to maintain the uniform crystallization of overall particles, in order to avoid hollow or local particle damage. Hitherto, the successful conversion to binder-free zeolites with a well-retained shape was mainly reported for ZSM-5.[31−33] Recently, we realized the synthesis of MOR spheres with good mechanical strength,[34] in which the precursor preparation with homogeneous elemental distribution was revealed to be essential for avoiding surface cracks or hollow cores. Moreover, to reduce the difficulty for complete conversion, a large amount of zeolite powder was also added for the preparation of a preshaped precursor,[35,36] which allows better control of the product property, but increases the complexity of the whole procedure.

In this paper, mechanically robust spherical ferrierite in millimeter size was successfully synthesized via vapor-assisted conversion of Na and Al doped commercial silica spheres under the help of cheap ethylenediamine (EDA). The resultant spheres have a well-retained shape, and the ferrierite content can reach as high as 100%. The physicochemical properties of the binder-free ferrierite spheres were characterized in detail, and the influence factors on the synthesis were investigated.

2. EXPERIMENTAL SECTION

2.1. Materials. The chemicals used for the synthesis included: porous silica spheres (SiO_2, 98.5 wt %, Qingdao Shiji Haiyang Desiccant Co., Ltd.), sodium aluminate ($NaAlO_2$, containing 51 wt % Al_2O_3 and 45 wt % Na_2O, Sinopharm Chemical Reagent Co., Ltd.), sodium hydroxide (NaOH, 96 wt %, Sinopharm Chemical Reagent Co., Ltd.), ethylenediamine (EDA, 99 wt %, Tianjin Damao Chemical Reagent Factory), and silica sol (30 wt %, Qingdao Chengyu Chemical Co., Ltd.). The reagents were used for the synthesis without further purification.

2.2. Preparation of Spherical Ferrierite. The spherical ferrierite was synthesized by the vapor-assisted transformation method. Typically, sodium aluminate was added into the deionized water to obtain a clear aqueous solution by magnetic stirring. The molar composition of the obtained impregnation solution was 1.0 Al_2O_3: 1.5 Na_2O: 75 H_2O. Then about 2 g of porous silica spheres was added into the impregnation solution (mass ratio of liquid to solid is 3/1) under vacuum conditions (~5000 Pa) for 10 min at room temperature, followed by filtering the excessive liquid and drying at ambient temperature to obtain the spherical precursors. 3.03 g EDA and 2.16 g water were put into the bottom of the stainless-steel autoclave, and then the precursors were transferred into a Teflon cup, which was placed above the liquid, so that the precursors did not contact the liquid during the crystallization. The autoclave was heated at 175 °C for 76 h under autogenous pressure. After crystallization, the spherical product was collected, washed with deionized water until the pH value was closed to 7, and dried at 100 °C overnight. The as-synthesized product was denoted as FER-S. The H-form product (denoted as H-FER-S) was obtained by calcination at 550 °C in air to remove the organic compounds.

For investigating the crystallization process of spherical ferrierite, spherical precursors were prepared and crystallized with the same procedure as FER-S except that the molar composition of impregnation solution for the precursors was 1.0 Al_2O_3: 1.5 Na_2O: 65 H_2O.

The OSDAs explored for the synthesis included tetrahydrofuran, pyridine, cyclohexylamine, and EDA. The preparation process of the precursors was similar to that of FER-S. All the precursors were impregnated by using the same solution (1.0 Al_2O_3: 1.5 Na_2O: 50 H_2O), and the OSDA (0.05 mol) and H_2O (0.1 mol) in the liquid phase for crystallization were kept at the same moles. The crystallization condition was the same as that of FER-S.

To learn the effect of the concentration and alkalinity of the impregnation solution on the synthesis, the precursors were prepared

https://doi.org/10.1021/acs.cgd.2c01486
Cryst. Growth Des. 2023, 23, 1951−1958

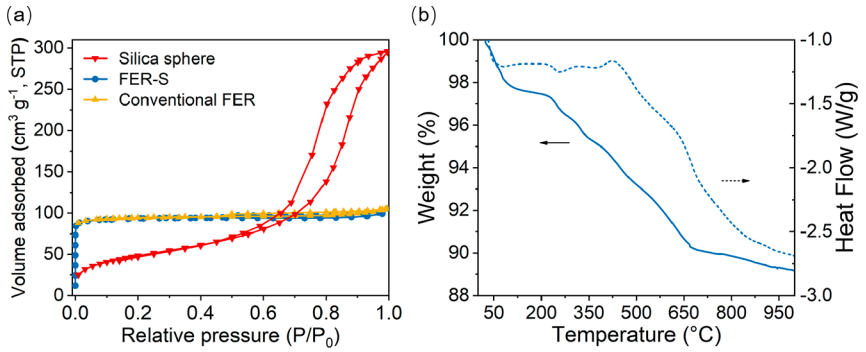

Figure 2. (a) N_2 adsorption−desorption isotherms of silica sphere (red), FER-S (blue), and conventional ferrierite (yellow). (b) Thermal analysis curves of FER-S.

Table 1. Elemental Compositions and Textual Properties of the Precursors and the Synthesized Products

		Si/Al/Na ratio[a]						
sample	x[b]	precursor	product	S_{BET}(m^2 g^{-1})	S_{micro}(m^2 g^{-1})	V_{total}(cm^3 g^{-1})	V_{micro}(cm^3 g^{-1})	R_z[c] (%)
conventional FER	-	-	-	315.4	283.5	0.16	0.13	-
1	45	1/0.087/0.130	1/0.089/0	289.5	259.1	0.15	0.12	92
2 (FER-S)	75	1/0.064/0.104	1/0.066/0	305.3	283.5	0.15	0.13	100
3	90	1/0.057/0.103	1/0.057/0	277.3	259.6	0.15	0.12	92
4	120	1/0.048/0.077	1/0.050/0.003	163.6	120.6	0.11	0.06	43
silica sphere	-	-	-	176.0	5.4	0.46	0	-

[a]Determined by XRF. [b]Impregnation solution for precursor preparation: 1.0 Al_2O_3: 1.5 Na_2O: xH_2O; [c]Zeolite content, which was calculated by comparing the micropore area of spherical product with that of conventional ferrierite.

by changing the water content of the impregnation solution (1.0 Al_2O_3: 1.5 Na_2O: x H_2O, where x = 45−120) and by varying the NaOH amount of the solution (1.0 Al_2O_3: x Na_2O: 65 H_2O, where x = 1.75−2.50), respectively. The crystallization condition was the same as that of FER-S.

2.3. Preparation of Conventional Ferrierite. 88.88 g silica sol, 4.65 g $NaAlO_2$, 0.93 g NaOH, 16.19 g EDA, and 100 g deionized water were mixed and stirred for 2 h. The mixture was transferred into a Telfon-lined stainless steel autoclave and heated at 170 °C for 60 h. The solid product was washed with deionized water several times. The product Si/Al ratio determined by XRF was 8.4.

2.4. Characterization. The crystalline phases of the products were determined by powder X-ray diffraction (XRD) on a PANalytical X'Pert PRO X-ray diffractometer with Cu Kα radiation (λ = 0.154059 nm). The elemental composition was characterized by a Philips Magix-601 X-ray fluorescence (XRF) spectrometer. The product morphology was observed using a Hitachi SU8020 scanning electron microscope (for all SEM images except Figure 1d) and Hitachi TM3000 (for Figure 1d only). N_2 adsorption and desorption isotherms were measured on Micromeritics ASAP 2020 analyzer at −196 °C. Prior to the analysis, samples were pretreated at 300 °C under a vacuum for 5 h. The total surface area was calculated from the BET equation. The micropore area and micropore volume were evaluated by the t-plot method. The acidity was measured by temperature-programmed desorption of ammonia (NH_3-TPD) on a Micromeritics Autochem II 2920. 100 mg of H-form sample was first outgassed in He (60 mL min^{-1}) at 650 °C for 1 h. After cooling to 100 °C, the sample started to adsorb NH_3 under a flow of NH_3/He for 1 h and purged by He until the baseline was stable. The desorption was carried out from 100 to 650 °C under He (20 mL min^{-1}) with a heating rate of 10 °C min^{-1}. The compressive strength of the samples was measured on ZQJ-II Intelligent particle strength tester produced by Dalian Intelligent Testing Instrument Co. Ltd. The solid-state MAS NMR spectra were recorded on a Bruker Avance III 600 spectrometer with a magnetic field intensity of 14.1 T, using a 4 mm WVT double resonances MAS probe. The ^{29}Si MAS NMR spectra were recorded at a resonance frequency of 119.2 MHz with a spinning rate of 8 kHz and a pulse width of 2.5 μs. The recycle delay was 10 s. The ^{27}Al MAS NMR spectra were recorded at 156.3 MHz with a spinning rate of 12 kHz and 2 s recycle delay. Thermal analysis (TA) experiments were conducted on a SDT Q600 thermal analyzer. About 10 mg sample was used and heated from room temperature to 1000 °C at a rate of 10 °C min^{-1} in air with a flow rate of 100 mL min^{-1}.

3. RESULTS AND DISCUSSION

3.1. Synthesis and Characterization of Spherical Ferrierite Zeolite. Millimeter-sized spherical ferrierite zeolite (named FER-S) was synthesized by a vapor-assisted transformation method using Na and Al doped amorphous silica spheres as precursors and EDA aqueous solution as the liquid phase. The crystallization was carried out at 175 °C for 76 h. The powder XRD patterns of the samples are shown in Figure 1a,b. The pristine silica spheres were amorphous with a broad peak between 15 and 30°. The XRD pattern of the spherical product was in good agreement with the simulated pattern of the FER phase, evidencing the good crystallinity of the product. Figure 1c presents the optical photograph of the as-synthesized FER-S, showing that the spherical shape with a size of about 2 mm is well maintained after crystallization. No breakage or cracking can be observed. The cross-section image in Figure 1d evidences the solid interior of the sphere. Further magnification of the interior (Figure 1e) reveals that ferrierite crystals are in plate-like morphology, and they are interwoven with each other. We further measured the mechanical strength of the calcined spherical FER-S. A high average compressive strength of 32 N was obtained, which should result from the solid interior of the spheres and the compact crystal intergrowth.

Figure 2a gives the N_2 adsorption and desorption isotherms of the samples. The spherical FER-S is a typical microporous material with type I isotherm. The BET surface area is 305 m^2 g^{-1}, and the micropore surface area is 283 m^2 g^{-1}. The values are close to those of conventional ferrierite powder synthesized

https://doi.org/10.1021/acs.cgd.2c01486
Cryst. Growth Des. 2023, 23, 1951−1958

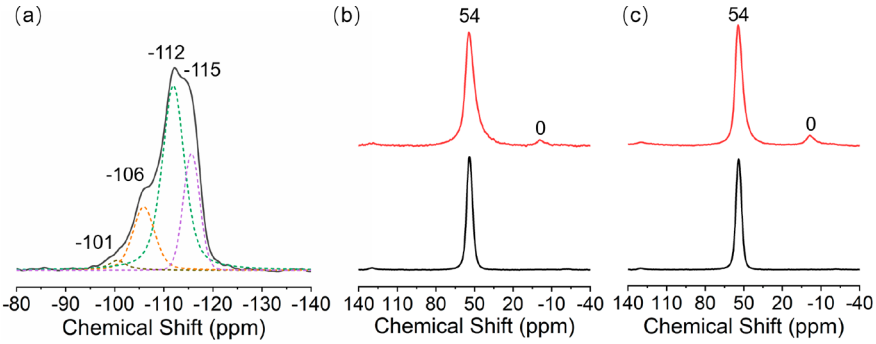

Figure 3. (a) ^{29}Si and (b) ^{27}Al MAS NMR spectra of spherical FER-S. (c) ^{27}Al MAS NMR spectra of conventional ferrierite. Black line: as-synthesized sample. Red line: calcined sample.

by a conventional method (Table 1). To confirm the origin of the micropores in FER-S, the textural properties of the pristine silica sphere were also determined. A type IV isotherm was obtained, giving a large external area and mesopore volume, but a very small micropore area. Therefore, we evaluate the zeolite content in FER-S by comparing its micropore area with that of conventional ferrierite. Note that the relative XRD crystallinity of zeolites is not used for the evaluation herein, as it is sensitive to the crystal morphology, size, and occluded substances of the samples, especially for the low-angle peaks. The result in Table 1 indicated that the precursor was completely transformed into ferrierite zeolite. Such a high ferrierite content in the shaped product has never been reported before, which would be favorable for its catalytic applications.

According to the XRF results (Table 1), the spherical FER-S has a Si/Al molar ratio of 15.3, and no Na ions were detected, meaning that H-form ferrierite can be directly obtained by simple calcination without an ion exchange process. The thermal analysis curves are shown in Figure 2b. In combination with the XRF and TG results, the unit cell composition of as-synthesized FER-S can be determined to be $EDA_{3.30}(H_2O)_{3.50}|[Al_{2.21}Si_{33.79}O_{72}]$, showing that only part of EDA was protonated in the crystals to balance the negative framework.

The ^{29}Si and ^{27}Al MAS NMR spectra of the as-synthesized FER-S and its calcined one are shown in Figure 3. There are four coordination environments observed for Si atoms with chemical shifts at −101, −106, −112, and −115 ppm. Both signals at −112 and −115 ppm can be attributed to the Si(0Al) species due to the existence of four T atom sites in the FER framework.[37] The signal at −106 ppm corresponds to Si(1Al) species. The weak signal at −101 ppm may be associated with Si(1Al) of different T sites or Si(OH) species. The ^{27}Al MAS NMR spectrum of the as-synthesized FER-S gives one narrow strong resonance at 54 ppm, evidencing that all the Al atoms exist in the framework in a tetrahedral coordination environment. After calcination, a weak signal at 0 ppm appears in the spectrum, which implies the occurrence of dealumination during calcination, similar to that of conventional ferrierite.

The acid properties of the directly calcined FER-S (namely H-FER-S) were characterized by NH_3-TPD. As shown in Figure 4, there are two desorption peaks around 210 and 472 °C, corresponding to the weak and strong acid sites, respectively. Based on the high-temperature desorption peak, the acid amount in H-FER-S was calculated to be 0.51 mmol g^{-1}.

3.2. Crystallization Process Investigation. The crystallization process of spherical FER was investigated (the molar composition of the impregnation solution was 1.0 Al_2O_3: 1.5 Na_2O: 65 H_2O), and the results are shown in Figure 5. From the XRD patterns of the samples with different crystallization times (Figure 5a), no obvious diffraction peak can be observed for the 12 h sample. After crystallization for 24 h, a small peak at 9.3° appears, indicating the generation of a small amount of ferrierite crystals in the product. When the crystallization time prolongs to 36 h, the characteristic peaks belonging to the FER phase can be clearly observed together with a weak broad peak at 20−30°, implying the existence of amorphous materials in the solid product. After 48 h, the diffraction peaks of the FER phase got stronger, and the broad peak became indistinguishable. The crystallinity of the samples showed little change after 60 h until the end of the crystallization.

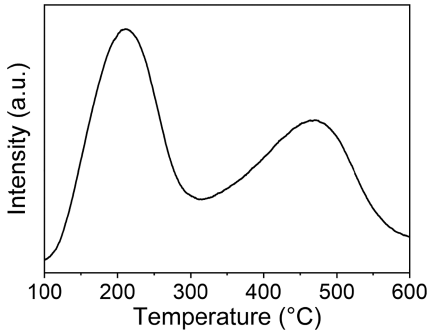

Figure 4. NH_3-TPD curve of the spherical H-FER-S sample.

The SEM images of the samples are presented in Figure 5b. The interior of the initial spheres consists of nanoparticles (about 50 nm) with irregular morphology. Following the progress of crystallization, these aggregated particles grow gradually. A small amount of lamellar crystals can be observed for the 36 h sample. Subsequently, the amount of lamellar crystals increases at the expense of amorphous materials. For the 72 h sample, the product is completely crystallized with plate-like morphology. The morphology evolution of the samples is in agreement with the XRD results.

3.3. Effect of OSDA Type and Precursor Compositions on the Synthesis of Spherical Ferrierite. The effect of OSDA type on the synthesis is displayed in Figure 6. All the OSDAs selected here were previously reported to be effective for the conventional hydrothermal synthesis of ferrierite. It is clear that EDA possessed the best ability for the synthesis of ferrierite. With the use of pyridine as OSDA, a large amount of MOR was observed together with the formation of ferrierite. When using cyclohexylamine as OSDA, the major phase of the product became MOR. For tetrahydrofuran, only amorphous

https://doi.org/10.1021/acs.cgd.2c01486
Cryst. Growth Des. 2023, 23, 1951−1958

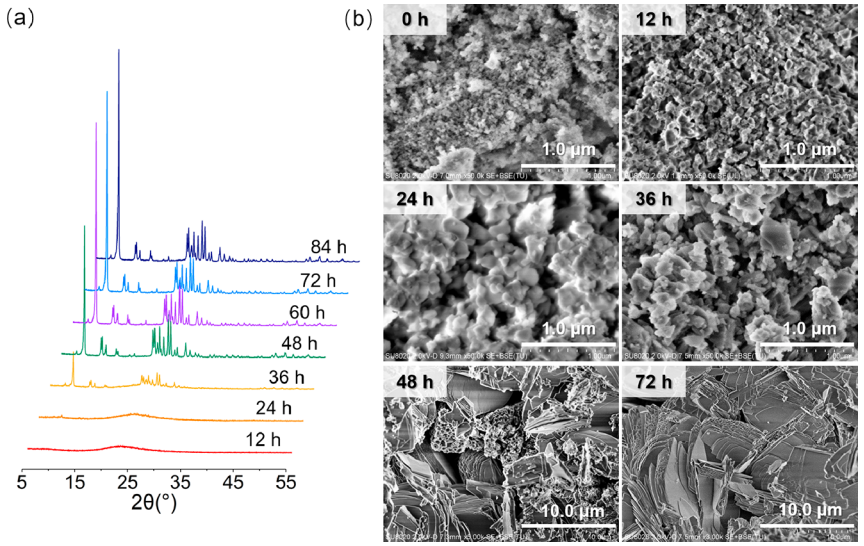

Figure 5. XRD patterns (a) and SEM images (b) of the spherical FER-S with different crystallization times.

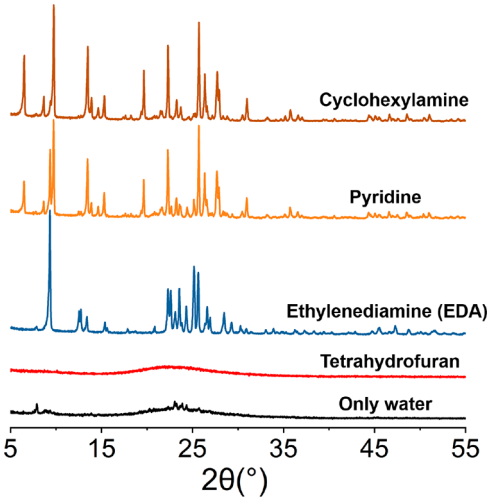

Figure 6. XRD patterns of the products synthesized by vapor-assisted conversion with the use of different OSDAs in the liquid phase.

product was obtained, which was similar to the results of pure water as the liquid phase and suggests the weak directing ability of tetrahydrofuran.

The precursor compositions also have an important influence on the synthesis of spherical ferrierite. Four silica-based precursors were first prepared by changing the water content of impregnation solution (1.0 Al_2O_3: 1.5 Na_2O: x H_2O, where x = 45, 75, 90, 120). As listed in Table 1, following the decrease of impregnation solution concentration, both the Si/Al ratio and Si/Na ratio of the prepared precursors rose significantly. The Na/Al ratio of the precursor varied in the range of 1.45−1.79, which was close to that of the impregnation solution, showing that the variation of solution concentration has little effect on the deposition of Al and Na on the precursor under the investigated conditions.

The XRD patterns and textural properties of the synthesized products are displayed in Table 1 and Figure 7a, respectively. Samples 1, 2, and 3 possessed high crystallinity, and their zeolite contents were more than 90%, while for sample 4 prepared using the precursor with the lowest impregnation solution concentration, its crystallinity was low and the corresponding zeolite content was only 43%. Given that EDA can direct the synthesis of ferrierite in a wide range of Si/

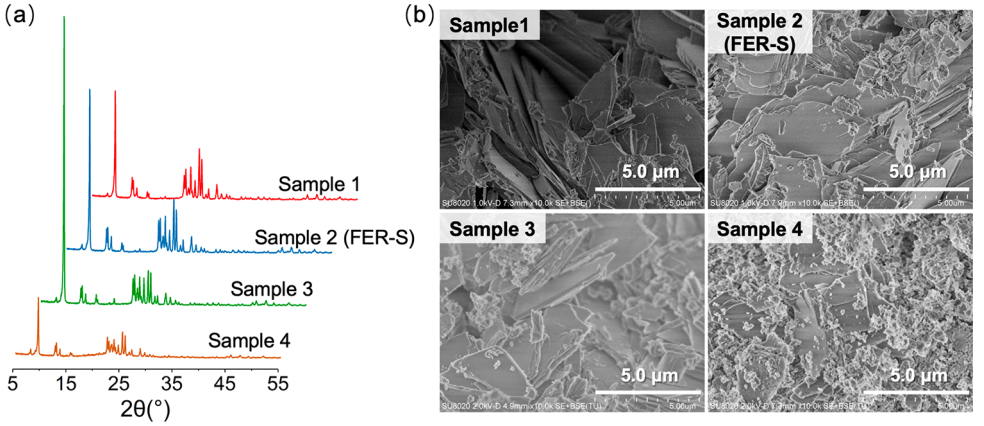

Figure 7. Effect of precursors prepared with different impregnation solution concentrations on the synthesis. (a) XRD patterns and (b) SEM images.

https://doi.org/10.1021/acs.cgd.2c01486
Cryst. Growth Des. 2023, 23, 1951−1958

Al ratios,[38] the low crystallinity of sample 4 was supposed to be caused by the lower Na content on the precursor. Moreover, all four products maintained their spherical shape after crystallization. From Figure 7b, the ferrierite crystals have plate-like morphology, and there are obvious amorphous residues for sample 4, which are consistent with the results of XRD and N_2 physisorption. The elemental compositions of the products are given in Table 1, indicating that the Si/Al ratio of the products was close to that of the precursors and there were no Na ions in the three well-crystallized ferrierite products.

The effect of impregnation solution alkalinity on the synthesis was investigated by varying the NaOH amount of the solution (1.0 Al_2O_3: xNa_2O: 65 H_2O, where x = 1.75, 2.00, 2.50). The correspondingly synthesized products were named as sample 5, 6, and 7 respectively. As shown in Table 2, the three precursors possessed a similar Si/Al ratio, and the Na/Al ratio of the precursors showed a rising trend following the increase of impregnation solution alkalinity. It is noted that for the precursor of sample 7, its Na/Al ratio was obviously lower than that of the impregnation solution, implying that the relatively less deposition of Na than Al on the precursor when using high alkalinity solution.

Table 2. Elemental Compositions of the Precursors and the Products

		Si/Al/Na ratio[a]	
sample	x[b]	precursor	product
5	1.70	1/0.070/0.123	1/0.07/0
6	2.00	1/0.071/0.133	1/0.072/0.004
7	2.50	1/0.072/0.147	1/0.069/0.003

[a]Determined by XRF. [b]Impregnation solution for precursor preparation: 1.0 Al_2O_3: xNa_2O: 65 H_2O.

The XRD patterns and SEM images of the samples are shown in Figure 8. When x = 1.75, the sample was pure FER phase. Increasing x to 2, quartz impurity with characteristic peak at 20.8° appeared in the XRD pattern, which grew stronger following the increase of solution alkalinity. The change of impregnation solution alkalinity also affected the crystal morphology of the samples, although they all maintained the spherical shape. The crystals were plate-like at x = 1.75. Their thickness became thinner when x = 2. Further increasing the solution alkalinity, the crystals morphology became irregular together with the existence of amorphous materials. Moreover, from Table 2, the Si/Al ratio of the products resembled that of the precursors, but a small amount of Na ions was left on samples 6 and 7. These results demonstrated that the Na amount on the precursors, which was determined by the concentration and alkalinity of impregnation solution, has important effects on the ferrierite crystallization and its product purity. To keep the Na/Si ratio of the precursor in the range of 0.10−0.13 would facilitate the synthesis of pure FER product with no Na residues.

4. CONCLUSIONS

Millimeter-sized binder-free spherical ferrierite zeolite has been successfully synthesized by vapor-assisted conversion of Na and Al doped amorphous silica spheres. EDA was demonstrated to be powerful OSDA for the synthesis under the investigated conditions. The conversion of the precursor can be complete, achieving about 100% ferrierite content in the resultant spheres. The well-maintained shape together with solid interior and compact crystals intergrowth was believed to contribute to the good mechanical strength of the product. As Na^+ ions did not incorporate in the as-synthesized spherical product, proton-form ferrierite spheres can be obtained after simple calcination, which would be favorable for its catalytic applications. The Na amount on the precursor spheres was revealed to have important effects on the ferrierite crystallization and phase purity, and the optimum Na/Si ratio was in the range of 0.10−0.13. It is anticipated that this facile method will benefit the preparation of more industrially important binder-free zeolite spheres.

AUTHOR INFORMATION

Corresponding Authors

Peng Tian − *National Engineering Research Center of Lower-Carbon Catalysis Technology, Dalian Institute of Chemical Physics, Chinese Academy of Sciences, Dalian 116023, People's Republic of China; University of Chinese Academy of Sciences, Beijing 100049, People's Republic of China*; Email: tianpeng@dicp.ac.cn

Zhongmin Liu − *National Engineering Research Center of Lower-Carbon Catalysis Technology, Dalian Institute of Chemical Physics, Chinese Academy of Sciences, Dalian 116023, People's Republic of China; University of Chinese Academy of Sciences, Beijing 100049, People's Republic of China*; Email: zml@dicp.ac.cn

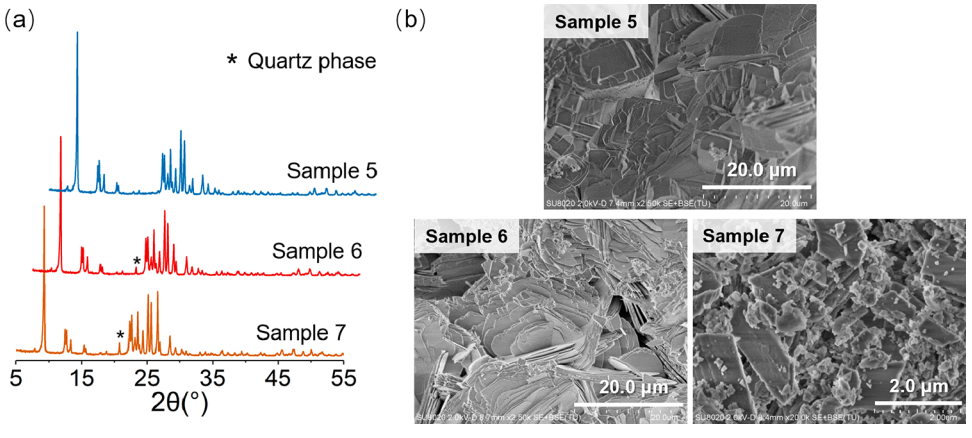

Figure 8. Effect of precursors prepared with different impregnation solution alkalinity on the synthesis. (a) XRD patterns and (b) SEM images.

https://doi.org/10.1021/acs.cgd.2c01486
Cryst. Growth Des. 2023, 23, 1951−1958

Authors

Lingyun Li − *National Engineering Research Center of Lower-Carbon Catalysis Technology, Dalian Institute of Chemical Physics, Chinese Academy of Sciences, Dalian 116023, People's Republic of China; University of Chinese Academy of Sciences, Beijing 100049, People's Republic of China;* orcid.org/0000-0003-3868-6389

Quanyi Wang − *National Engineering Research Center of Lower-Carbon Catalysis Technology, Dalian Institute of Chemical Physics, Chinese Academy of Sciences, Dalian 116023, People's Republic of China*

Dong Fan − *National Engineering Research Center of Lower-Carbon Catalysis Technology, Dalian Institute of Chemical Physics, Chinese Academy of Sciences, Dalian 116023, People's Republic of China*

Miao Yang − *National Engineering Research Center of Lower-Carbon Catalysis Technology, Dalian Institute of Chemical Physics, Chinese Academy of Sciences, Dalian 116023, People's Republic of China*

Complete contact information is available at: https://pubs.acs.org/10.1021/acs.cgd.2c01486

Author Contributions

The manuscript was written through contributions of all authors. All authors have given approval to the final version of the manuscript.

Notes

The authors declare no competing financial interest.

■ ACKNOWLEDGMENTS

The authors gratefully acknowledge the National Natural Science Foundation of China (No. 21991090, 21991091, 22171259, 22272173).

■ REFERENCES

(1) Long, Y. C.; Ma, M. H.; Sun, Y. J.; Jiang, H. W. Synthesis, Ion-exchange, Structural Characterization and Adsorption of K, Na-FER Type Zeolite. *J. Incl. Phenom. Macrocycl. Chem.* **2000**, *37* (1), 103−120.

(2) Xu, H.; Zhu, J.; Zhu, L. F.; Zhou, E. M.; Shen, C. Advances in the Synthesis of Ferrierite Zeolite. *Molecules* **2020**, *25* (16), 3722.

(3) Khitev, Y. P.; Ivanova, I. I.; Kolyagin, Y. G.; Ponomareva, O. A. Skeletal isomerization of 1-butene over micro/mesoporous materials based on FER zeolite. *Appl. Catal., A* **2012**, *441*−*442*, 124−135.

(4) Ham, H.; Jung, H. S.; Kim, H. S.; Kim, J.; Cho, S. J.; Lee, W. B.; Park, M.-J.; Bae, J. W. Gas-Phase Carbonylation of Dimethyl Ether on the Stable Seed-Derived Ferrierite. *ACS Catal.* **2020**, *10* (9), 5135−5146.

(5) Margarit, V. J.; Díaz-Rey, M. R.; Navarro, M. T.; Martínez, C.; Corma, A. Direct Synthesis of Nano-Ferrierite along the 10-Ring-Channel Direction Boosts Their Catalytic Behavior. *Angew. Chem., Int. Ed.* **2018**, *57* (13), 3459−3463.

(6) Jung, H. S.; Zafar, F.; Wang, X.; Nguyen, T. X.; Hong, C. H.; Hur, Y. G.; Choung, J. W.; Park, M.-J.; Bae, J. W. Morphology Effects of Ferrierite on Bifunctional Cu−ZnO−Al_2O_3/Ferrierite for Direct Syngas Conversion to Dimethyl Ether. *ACS Catal.* **2021**, *11* (22), 14210−14223.

(7) Yu, Q.; Richter, M.; Kong, F. X.; Li, L. D.; Wu, G. J.; Guan, N. J. Selective catalytic reduction of NO by hydrogen over Pt/ZSM-35. *Catal. Today* **2010**, *158* (3), 452−458.

(8) Lee, Y.; Park, M. B.; Kim, P. S.; Vicente, A.; Fernandez, C.; Nam, I.-S.; Hong, S. B. Synthesis and Catalytic Behavior of Ferrierite Zeolite Nanoneedles. *ACS Catal.* **2013**, *3* (4), 617−621.

(9) Xu, H.; Yu, Y.; Zhu, L. F.; Bian, C. Q.; Zhai, H. L.; Tong, J. Y.; Wu, H. Z.; Shen, C. Preparation of Aluminosilicate Ferrierite Zeolite Nanosheets with Controllable Thickness in the Presence of a Sole Organic Structure Directing Agent. *Molecules* **2020**, *25* (4), 771.

(10) Pinar, A. B.; Gómez-Hortigüela, L.; McCusker, L. B.; Pérez-Pariente, J. Controlling the Aluminum Distribution in the Zeolite Ferrierite via the Organic Structure Directing Agent. *Chem. Mater.* **2013**, *25* (18), 3654−3661.

(11) Kibby, C. L.; Perrotta, A. J.; Massoth, F. E. Composition and catalytic properties of synthetic ferrierite. *J. Catal.* **1974**, *35* (2), 256−272.

(12) Guo, G. Q.; Sun, Y. J.; Long, Y. C. Synthesis of FER type zeolite with tetrahydrofuran as the template. *Chem. Commun.* **2000**, *19*, 1893−1894.

(13) Ahedi, R. K.; Kotasthane, A. N.; Rao, B. S.; Manna, A.; Kulkarni, B. D. Synthesis of Ferrierite-Type Zeolite in the Presence of a Catalytic Amount of Pyrrolidine and Sodium Bis(2-ethyhlhexyl) Sulfosuccinate. *J. Colloid Interface Sci.* **2001**, *236* (1), 47−51.

(14) Wei, P. F.; Zhu, X. X.; Wang, Y. N.; Chu, W. F.; Xie, S. J.; Yang, Z. Q.; Liu, X. B.; Li, X. J.; Xu, L. Y. Rapid synthesis of ferrierite zeolite through microwave assisted organic template free route. *Microporous Mesoporous Mater.* **2019**, *279*, 220−227.

(15) Matsufuji, T.; Nishiyama, N.; Ueyama, K.; Matsukata, M. Crystallization of ferrierite (FER) on a porous alumina support by a vapor-phase transport method. *Microporous Mesoporous Mater.* **1999**, *32* (1), 159−168.

(16) Zhao, Z. C.; Zhang, W. P.; Ren, P. J.; Han, X. W.; Müller, U.; Yilmaz, B.; Feyen, M.; Gies, H.; Xiao, F. S.; De Vos, D.; et al. Insights into the Topotactic Conversion Process from Layered Silicate RUB-36 to FER-type Zeolite by Layer Reassembly. *Chem. Mater.* **2013**, *25* (6), 840−847.

(17) Wang, L.; Xu, H. Y.; Yan, N. N.; Correll, S.; Xu, S. T.; Guo, P.; Tian, P.; Liu, Z. M. Exploring Brønsted acids confined in the 10-ring channels of the zeolite ferrierite. *CrystEngComm* **2018**, *20* (6), 699−702.

(18) Román-Leshkov, Y.; Moliner, M.; Davis, M. E. Impact of Controlling the Site Distribution of Al Atoms on Catalytic Properties in Ferrierite-Type Zeolites. *J. Phys. Chem. C* **2011**, *115* (4), 1096−1102.

(19) Pinar, A. B.; Verel, R.; Pérez-Pariente, J.; van Bokhoven, J. A. Direct evidence of the effect of synthesis conditions on aluminum siting in zeolite ferrierite: A ^{27}Al MQ MAS NMR study. *Microporous Mesoporous Mater.* **2014**, *193*, 111−114.

(20) Dedecek, J.; Lucero, M. J.; Li, C. B.; Gao, F.; Klein, P.; Urbanova, M.; Tvaruzkova, Z.; Sazama, P.; Sklenak, S. Complex Analysis of the Aluminum Siting in the Framework of Silicon-Rich Zeolites. A Case Study on Ferrierites. *J. Phys. Chem. C* **2011**, *115* (22), 11056−11064.

(21) Plank, C. J.; Rosinski, E. J.; Rubin, M. K.Synthetic crystalline zeolite contg. nitrogen-contg. cation derived from ethylene diamine or pyrrolidine. US4016245-A, 1974.

(22) Xu, W. Y.; Li, J. Q.; Li, W. Y.; Zhang, H. M.; Liang, B. C. Nonaqueous synthesis of ZSM-35 and ZSM-5. *Zeolites* **1989**, *9* (6), 468−473.

(23) Dai, W. J.; Ruaux, V.; Deng, X.; Tai, W. S.; Wu, G. J.; Guan, N. J.; Li, L. D.; Valtchev, V. Synthesis and catalytic application of nanorod-like FER-type zeolites. *J. Mater. Chem. A* **2021**, *9* (44), 24922−24931.

(24) Pinar, A. B.; Gomez-Hortiguela, L.; Perez-Pariente, J. Cooperative Structure Directing Role of the Cage-Forming Tetramethylammonium Cation and the Bulkier Benzylmethylpyrrolidinium in the Synthesis of Zeolite Ferrierite. *Chem. Mater.* **2007**, *19* (23), 5617−5626.

(25) Wang, S.; Bai, P.; Sun, M. Z.; Liu, W.; Li, D. D.; Wu, W. Z.; Yan, W. F.; Shang, J.; Yu, J. H. Fabricating Mechanically Robust Binder-Free Structured Zeolites by 3D Printing Coupled with Zeolite Soldering: A Superior Configuration for CO_2 Capture. *Adv. Sci.* **2019**, *6* (17), 1901317.

(26) Rodaum, C.; Klinyod, S.; Nunthakitgoson, W.; Chaipornchalerm, P.; Liwatthananukul, N.; Iadrat, P.; Wattanakit, C. Binder-free hierarchical zeolite pellets and monoliths derived from

ZSM-5@LDHs composites for bioethanol dehydration to ethylene. *Chem. Commun.* **2022**, *58* (69), 9618−9621.
(27) Lawson, S.; Newport, K.; Al-Naddaf, Q.; Ameh, A. E.; Rownaghi, A. A.; Petrik, L. F.; Rezaei, F. Binderless zeolite monoliths production with sacrificial biopolymers. *Chem. Eng. J.* **2021**, *407*, 128011.
(28) Tsai, R. F.; Du, K. J.; Cheng, T. Y.; Ho, G. H.; Wu, P. H.; Liu, S. B.; Tsai, T. C. Solid-state synthesis of mesoporous MFI zeolite from self-bonded silica pellets. *Catal. Today* **2013**, *204*, 30−37.
(29) He, Y.; Cui, X. M.; Liu, X. D.; Wang, Y. P.; Zhang, J.; Liu, K. Preparation of self-supporting NaA zeolite membranes using geopolymers. *J. Membr. Sci.* **2013**, *447*, 66−72.
(30) Mintova, S.; Hölzl, M.; Valtchev, V.; Mihailova, B.; Bouizi, Y.; Bein, T. Closely Packed Zeolite Nanocrystals Obtained via Transformation of Porous Amorphous Silica. *Chem. Mater.* **2004**, *16* (25), 5452−5459.
(31) Zhao, T. T.; Wang, Y. Q.; Sun, C.; Zhao, A. J.; Wang, C.; Zhang, X.; Zhao, J. J.; Wang, Z. Y.; Lu, J. X.; Wu, S. H.; et al. Direct synthesis of hierarchical binder-free ZSM-5 and catalytic properties for MTP. *Microporous Mesoporous Mater.* **2020**, *292*, 109731.
(32) Yue, M. B.; Yang, N.; Jiao, W. Q.; Wang, Y. M.; He, M. Y. Dry-gel synthesis of shaped binderless zeolites composed of nanosized ZSM-5. *Solid State Sci.* **2013**, *20*, 1−7.
(33) Peppel, T.; Paul, B.; Kraehnert, R.; Enke, D.; Lücke, B.; Wohlrab, S. Shape-preserving transformation of monolithic porous glass into MFI-type zeolite. *Microporous Mesoporous Mater.* **2012**, *158*, 180−186.
(34) Li, L. Y.; Wang, Q. Y.; Liu, H. C.; Sun, T. T.; Fan, D.; Yang, M.; Tian, P.; Liu, Z. M. Preparation of Spherical Mordenite Zeolite Assemblies with Excellent Catalytic Performance for Dimethyl Ether Carbonylation. *ACS Appl. Mater. Interfaces* **2018**, *10* (38), 32239−32246.
(35) Zhang, W. S.; Gao, S. Y.; Xie, S. J.; Liu, H.; Zhu, X. X.; Shang, Y. C.; Liu, S. L.; Xu, L. Y.; Zhang, Y. A shaped binderless ZSM-11 zeolite catalyst for direct amination of isobutene to tert-butylamine. *Chin. J. Catal.* **2017**, *38* (1), 168−175.
(36) Wang, D. J.; Liu, Z. N.; Wang, H.; Xie, Z. K.; Tang, Y. Shape-controlled synthesis of monolithic ZSM-5 zeolite with hierarchical structure and mechanical stability. *Microporous Mesoporous Mater.* **2010**, *132* (3), 428−434.
(37) Sarv, P.; Wichterlová, B.; Čejka, J. Multinuclear MQMAS NMR Study of NH4/Na-Ferrierites. *J. Phys. Chem. B* **1998**, *102* (8), 1372−1378.
(38) Pan, R. L.; Jia, M. J.; Li, Y. P.; Li, X. F.; Dou, T. In Situ Delamination of Ferrierite Zeolite and its Performance in the Catalytic Cracking of C4 Hydrocarbons. *Chin. J. Chem. Eng.* **2014**, *22* (11), 1237−1242.

https://doi.org/10.1021/acs.cgd.2c01486
Cryst. Growth Des. 2023, 23, 1951−1958